A dominant role of oxygen additive on cold atmospheric-pressure He + O2 plasmas

Aijun Yang, Dingxin Liu, Mingzhe Rong, Xiaohua Wang, and Michael G. Kong

Citation: Physics of Plasmas (1994-present) **21**, 083501 (2014); doi: 10.1063/1.4884787
View online: http://dx.doi.org/10.1063/1.4884787
View Table of Contents: http://scitation.aip.org/content/aip/journal/pop/21/8?ver=pdfcov
Published by the AIP Publishing

A dominant role of oxygen additive on cold atmospheric-pressure He + O_2 plasmas

Aijun Yang,[1] Dingxin Liu,[1,a)] Mingzhe Rong,[1] Xiaohua Wang,[1,a)] and Michael G. Kong[1,2,3]
[1]*Centre for Plasma Biomedicine, State Key Laboratory of Electrical Insulation and Power Equipment, Xi'an Jiaotong University, Xi'an 710049, People's Republic of China*
[2]*Frank Reidy Research Center for Bioelectrics, Old Dominion University, Norfolk, Virginia 23508, USA*
[3]*Department of Electrical and Computer Engineering, Old Dominion University, Norfolk, Virginia 23529, USA*

(Received 23 March 2014; accepted 29 May 2014; published online 1 August 2014)

We present in this paper how oxygen additive impacts on the cold atmospheric-pressure helium plasmas by means of a one-dimensional fluid model. For the oxygen concentration $[O_2] > \sim 0.1\%$, the influence of oxygen on the electron characteristics and the power dissipation becomes important, e.g., the electron density, the electron temperature in sheath, the electron-coupling power, and the sheath width decreasing by 1.6 to 16 folds with a two-log increase in $[O_2]$ from 0.1% to 10%. Also the discharge mode evolves from the γ mode to the α mode. The reactive oxygen species are found to peak in the narrow range of $[O_2] = 0.4\%$–0.9% in the plasmas, similar to their power-coupling values. This applies to their wall fluxes except for those of O* and O_2^-. These two species have very short lifetimes, thus only when generated in boundary layers within several micrometers next to the electrode can contribute to the fluxes. The dominant reactive oxygen species and the corresponding main reactions are schematically presented, and their relations are quantified for selected applications. © *2014 AIP Publishing LLC*. [http://dx.doi.org/10.1063/1.4884787]

I. INTRODUCTION

Most cold atmospheric-pressure plasmas (CAPs) are operated in a noble gas but usually with a small amount of molecular gases such as O_2 or N_2 to produce reactive oxygen species (ROS) and/or reactive nitrogen species (RNS). In particular, He + O_2 CAPs were extensively investigated in the last decade for various applications from material processing to biomedicine.[1–3] It is well known that the behaviors of CAPs in N_2 diluted by a noble gas is sensitive to the amount of N_2.[4,5] In comparison, the influence of O_2 additive is even more important due to (1) the strong electronegative nature of O_2 that changes the plasma features more significantly and (2) the production of ROS that is central to many important applications. Regards to the influence of O_2 additive on the helium CAPs, a lot of research has been reported in order to increase the ROS production efficiency and prevent plasma instability simultaneously.

In general, the maximal ROS production efficiency in He + O_2 CAPs is achieved when $[O_2]$=0.5%–3%.[6] It is demonstrated that the density of ground state atomic oxygen (O) peaks at $[O_2] \sim 0.6\%$ by the two-photon absorption laser induced fluorescence spectroscopy (TALIF) and the molecular beam mass spectroscopy (MBMS),[7,8] while the density of O_3 measured by MBMS keeps increase until the plasma extinguishes at very high O_2 fraction.[15] Similar density trends for such species have also been predicted by both the zero-dimensional global model and the one-dimensional fluid model.[9–11] However, the density trends of excited states of ROS, mainly the $O(^1D)$, $O(^1S)$, $O_2(a^1\Delta_g)$, and $O_2(b^1\sum_g^+)$, are still ambiguous. The peak point of emission spectral line at 777 nm ($O(3p^5P) \rightarrow O(3s^5S)$) varies from $[O_2] \sim 0.1\%$ to 1.5% in literature[12–15] probably because the density of $O(3p^5P)$ is sensitive to the discharge conditions, especially for the possible mixture of ambient air into the feeding gas. It is noted that the relative intensity of 777 nm spectral line may not reflect the density trends of $O(^1D)$ and $O(^1S)$, because the production/destruction mechanisms of these two species are much different to that of $O(3p^5P)$.[16] Besides, the dependences of O*($O(^1D)$ and $O(^1S)$) and O_2*($O_2(a^1\Delta_g)$ and $O_2(b^1\sum_g^+)$) densities on the oxygen concentration have also been predicted by numerical studies, but the results are somewhat different for different models.[10,11]

The main attention in previous studies was paid on the optimal O_2 concentration for ROS production, but the maximal density of a certain ROS might be inconsistent with its wall flux.[17–19] It is noted that the latter directly act on the treated targets thus reflects the "plasma dosage" for applications, but little has been known so far of its dependence on the O_2 fraction. Regarding the ROS production, the role of O_2 additive has been demonstrated mainly via plasma chemistry, but physically it may correspond to the power dissipation characteristics. The relationship between the power dissipation and the ROS production has little been reported before. Also, the O_2 additive may lead to the discharge mode (α and γ modes) transition due to its electronegative nature, and hence influence the plasma stability significantly.[20] All these are important for unraveling the dominant role of O_2 additive and regulating the He + O_2 CAPs for a specific application, and hence need further investigation.

a)Authors to whom correspondence should be addressed. Electronic addresses: liudingxin@gmail.com and xhw@mail.xjtu.edu.cn

In this paper, the impact of O_2 additive on the helium CAPs is investigated by means of a one-dimensional fluid model, for a large O_2 concentration spanning from 0% to 10%. The main purpose is to present the evolution of the discharge mode, the power dissipation, the ROS production chemistry, the densities and the wall fluxes of ROS, as well as the relationships among these features. The paper is organized as follows. The model used in the study is described briefly in Sec. II. The simulation results and discussions are presented in Sec. III. Finally, the conclusions are provided in Sec. IV.

II. DESCRIPTION OF THE MODEL

The one-dimensional fluid model used in this paper has been detailed in our previous studies,[17–19] and hence just briefly described here. The plasma source consists of two plane-parallel electrodes with a narrow separation of 2 mm and a large electrode width (to facilitate the use of one-dimensional model), similar to those used in experimental study.[21] The applied voltage has a radio-frequency sinusoidal waveform with a constant frequency of 13.56 MHz and a constant dissipated power density of 40 W/cm^3. The feeding gas is a He + O_2 mixture at the atmospheric pressure, with an oxygen content up to $[O_2] = 10\%$. The gas temperature is assumed to be 350 K based on the previous experimental study.[21]

The model incorporates 21 species and 267 reactions as referred from our previous global model.[10] More species and corresponding reactions are considered compared to our previous fluid models.[17–19] This leads to much heavier computational load, but on the other hand provides more precise results especially for the low density species like O_2^-. The 21 species include electron, positive ions (He^+, He_2^+, O^+, O_2^+, and O_4^+), negative ions (O^-, O_2^-, O_3^-, and O_4^-), electronic excited species (He* (He(2^3S) and He(2^1S)), He_2* ($He_2(a^3\sum_u^+)$), O*(O(^{1}D) and O(^{1}S)), and O_2*($O_2(a^1\Delta_g)$ and $O_2(b^1\sum_g^+)$), vibrational excited species ($O_2(\nu)$, $\nu = 1$-4), and grounded state neutrals (O, He, O_2, and O_3). Specifically, O, O*, O_2*, O_3, and O_2^- are known to be important in biology,[22] environmental science,[23,24] and surface engineering.[25]

The fluid model requires simultaneous solution of the drift-diffusion equation for each species, the electron energy equation and Poisson's equation, similar to the reports by other research groups.[26–30] The ion temperature is obtained using Wannier's formulation.[31] The transport coefficients for electrons and the electron-impact reaction rate coefficients are calculated as a function of the mean electron energy using Bolsig+, a Boltzmann solver.[32] The transport coefficients and the reaction rate coefficients for heavy species are detailed in our previous reports[10,17] and references therein.

The electrode loss of charged species takes into account the drift flux, the thermal flux, and the secondary emission of electrons. As stated in Ref. 17, the electrode loss of neutral species is given as

$$EL_i = p_i \Gamma_i s_e / V, \quad (1)$$

where EL_i represents the electrode loss of species i in the unit of cm^{-3} s^{-1}, p_i represents the loss probability of species i on the electrodes, s_e represents the total area (cm^2) of electrode-plasma interface, and V represents the volume of plasma (cm^3). The electrode losses of neutral species are correlate to their wall fluxes (thermal fluxes) which is focused in this paper, but it is difficult to get the p_i value due to the lack of knowledge of the adsorption/desorption of species as well as the surface reactions.[33] However, it is demonstrated in Ref. 17 that the electrode loss has little influence on the wall flux, and even it is constant when $p_i > 0.01$. So, in this paper, the p_i is set to be 0.01 for modelling study.

III. RESULTS AND DISCUSSIONS

A. Electron heating mechanisms

The impact of oxygen additive on the electron density, the electron temperature, and the electron generation rate of the He + O_2 CAP is shown in Fig. 1. The white curves in Fig. 1 represent the sheath boundaries. Compared to the pure helium plasma (the first row of subfigures), the impact of O_2 additive is little when $[O_2] \leq 0.1\%$, beyond that it becomes significant. This trend agrees well with the observation by Moravej *et al.* on the dependence of I-V curve on the O_2 concentration, noting that the I-V characteristic is mainly governed by electrons.[34] When the oxygen concentration increases from 0.1% to 10%, the sheath shrinks from 382 to

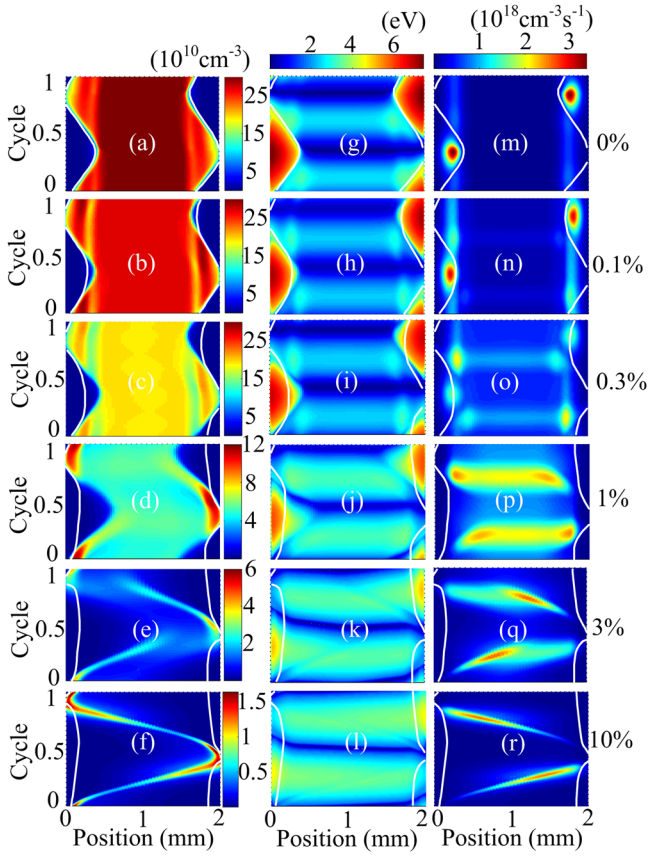

FIG. 1. Spatio-temporal evolution of electron density (a)-(f), electron temperature (g)-(l), and electron generation rate (m)-(r) at different oxygen concentrations. Each subfigure of electron density is normalized to its maximum value, while all the subfigures of electron temperature and electron generation rate are normalized to 7.4 eV and 3.34×10^{18} cm^{-3} s^{-1}, respectively. The white curves represent the sheath boundaries.

141 μm, the peak electron density decreases from 2.65×10^{11} to 1.62×10^{10} cm^{-3}, and the peak electron temperature (in the sheath) decreases from 7.05 to 4.48 eV. Changes of these plasma parameters are between 1.6 and 16 folds. Here, we consider the boundary of the sheath region to be determined by $n_- = 0.3n_+$, in which n_+ and n_- are the densities of positive and negative charged species, respectively. The sheath and the electron density boundaries overlap when $[O_2] \leq 0.1\%$, but become separated due to the increase of negative ions as the $[O_2]$ continues to increase.[35] Interestingly, the generation of electron dominates in the sheath when $[O_2] \leq 0.1\%$ (see Figs. 1(m) and 1(n)) but it changes in plasma bulk when $[O_2] \geq 0.3\%$ (see Figs. 1(o)–1(r)), which means that the plasma evolves from the γ mode into the α mode as the increase of O_2 concentration.[36] Since atmospheric pressure discharges in the α mode are more stable than in the γ mode, the power range for stable working is expanded.[20]

On the whole, the variations of electron density, electron temperature and discharge mode with oxygen concentration are mainly attributed to the enhancement of electronegativity. Here, the electronegativity (α) is defined as the ratio of anion density (n_a) to the electron density (n_e), i.e., $\alpha = n_a/n_e$. Higher oxygen concentration leads to higher density of O_3 through $O + O_2 + M \rightarrow O_3 + M$ and thus enhancing the electron attachment, primarily via $e + O_3 \rightarrow O^- + O_2$. Because the density of O_3 decreases from the centre to the electrodes,[17] the electron density decreases dramatically in the central region and hence it peaks at the bulk-sheath boundary when $[O_2] \geq 1\%$ (see Figs. 1(c)–1(f)). The decrease of electron density in plasma bulk leads to the increase of electric field to sustain the discharge current, and hence the electron temperature in plasma bulk increases (see Figs. 1(i)–1(l)). In contrary, the electron temperature in the sheath decreases due to the decrease of net charge density there. The main mechanisms for electron production are electron impact ionization and Penning ionization, both of which are sensitive to the electron temperature.[10] As a result, the electron heating is enhanced in the bulk region but reduced in the sheath, leading to the evolution from the γ mode to the α mode (see Figs. 1(m)–1(r)). Besides, the mode transition is also contributed by the electron detachment in bulk region, which has little relationship with electron temperature and therefore occupies a wide portion of a discharge cycle (see the distribution of electron generation in Fig. 1(p)).

B. Power dissipation

For low-pressure plasmas, it is reasonable to assume that all power dissipated in the discharge is absorbed by electrons.[37] As for atmospheric plasmas, however, the ions can also absorb much power directly from the electric field, especially for an electronegative discharge.[38] From the standpoint of plasma chemistry and applications relying on ROS/RNS, a large amount of dissipated power density in electrons is desirable for the production of reactive plasma species. Therefore, it is very important to investigate the dependence of power dissipation on oxygen concentration. As shown in Fig. 2(a), the power dissipation on ions (P_i) is almost invariant with oxygen concentration at about 20% of the total dissipated power when $[O_2] < 0.3\%$ and increases sharply when $[O_2] > 0.3\%$. By contrast, the power dissipation on electrons (P_e) decreases rapidly when $[O_2] > 0.3\%$. It is noted that the dependence of electronegativity on oxygen concentration is almost similar to that of P_i. According to our previous study,[19] the ratio of P_i to P_e ($\eta = P_i/P_e$) can be roughly estimated by

$$\eta = \frac{\mu_i(2\alpha + 1)}{\mu_e}, \tag{2}$$

where μ_e and μ_i are electron mobility and ion mobility, respectively. According to formula (2), it is no wonder that the partition of the dissipated power density between electrons and ions is closely related to electronegativity. For

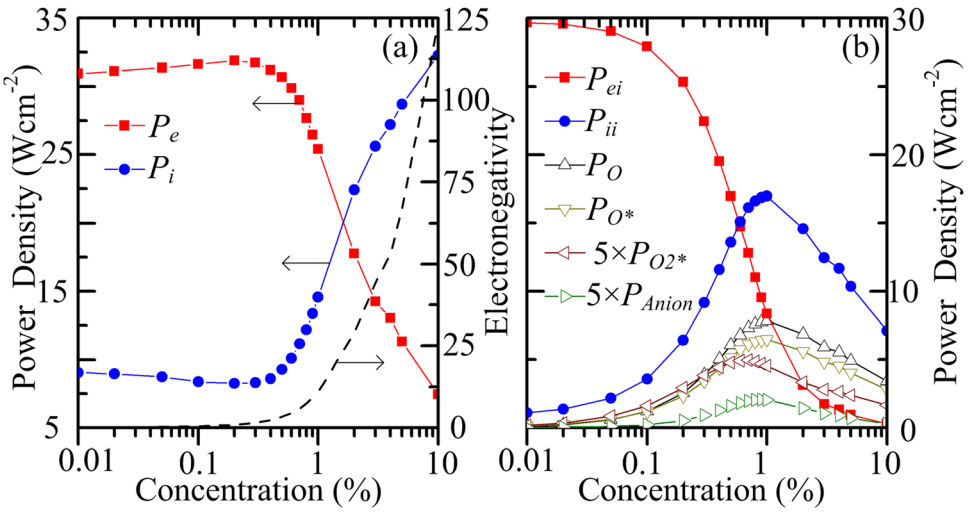

FIG. 2. Spatio-temporal averaged power densities coupled into electrons, ions, elastic collisions and several kinds of inelastic collisions as a function of oxygen concentration. P_e represents the power density coupled into electrons, P_i represents the ions, P_{ei} represents the elastic collisions, P_{ii} represents the inelastic collisions, P_O represents the generation of O, P_O* represents the generation of O*, P_{O2}* represents the generation of O_2*, and P_{Anion} represents the generation of anions.

example, the $\alpha = 30$ is obtained by numerical simulation when $[O_2] = 2\%$, so it is estimated by formula (2) that $\eta = 1.1$ with $\mu_e = 1100\,cm^2\ V^{-1}\ s^{-1}$ and $\mu_i = 20\,cm^2\ V^{-1}\ s^{-1}$. The estimation implies that P_i replaces P_e as the dominant role in the total dissipated power when $[O_2] > 2\%$, which is consistent with our numerical simulation (see Fig. 2(a)). When $[O_2] = 10\%$ at which the electronegativity is ~123, only 18% of input power is used for electron heating (P_e), indicating that such high oxygen concentration has low possibility to be efficient for the ROS production.

The power dissipation on electrons is consumed by elastic collisions (P_{el}) and inelastic collisions (P_{inel}). P_{el} is used to supply energy to the momentum transfer of electrons with the molecules and atoms of the feedstock gas, for example, $e + He \rightarrow e + He$ and $e + O_2 \rightarrow e + O_2$. Generally speaking, P_{inel} is desirable as it is used for reactive species production. Fig. 2(b) shows how the electron-coupling electrical power is partitioned onto elastic collisions, inelastic collisions, and ROS generation as well as their dependences on oxygen concentration. It can be found that more than 80% of input power is coupled by electrons when $[O_2] \leq 0.3\%$, but it is mainly consumed by elastic collisions which contribute little to the ROS production. The power density dissipated in elastic collisions decreases with the oxygen concentration, whereas the power dissipation on inelastic collisions of electrons increases with the oxygen concentration when $[O_2] < \sim 1\%$, and then decreases due to the decrease of P_e. The power dissipations on the production of O, O*(O(^{1}d) and O(^{1}s)), O_2*($O_2(a^1\Delta_g)$ and $O_2(b^1\sum_g^+)$), and anions (O^- and O_2^-) have similar trends with P_{inel},

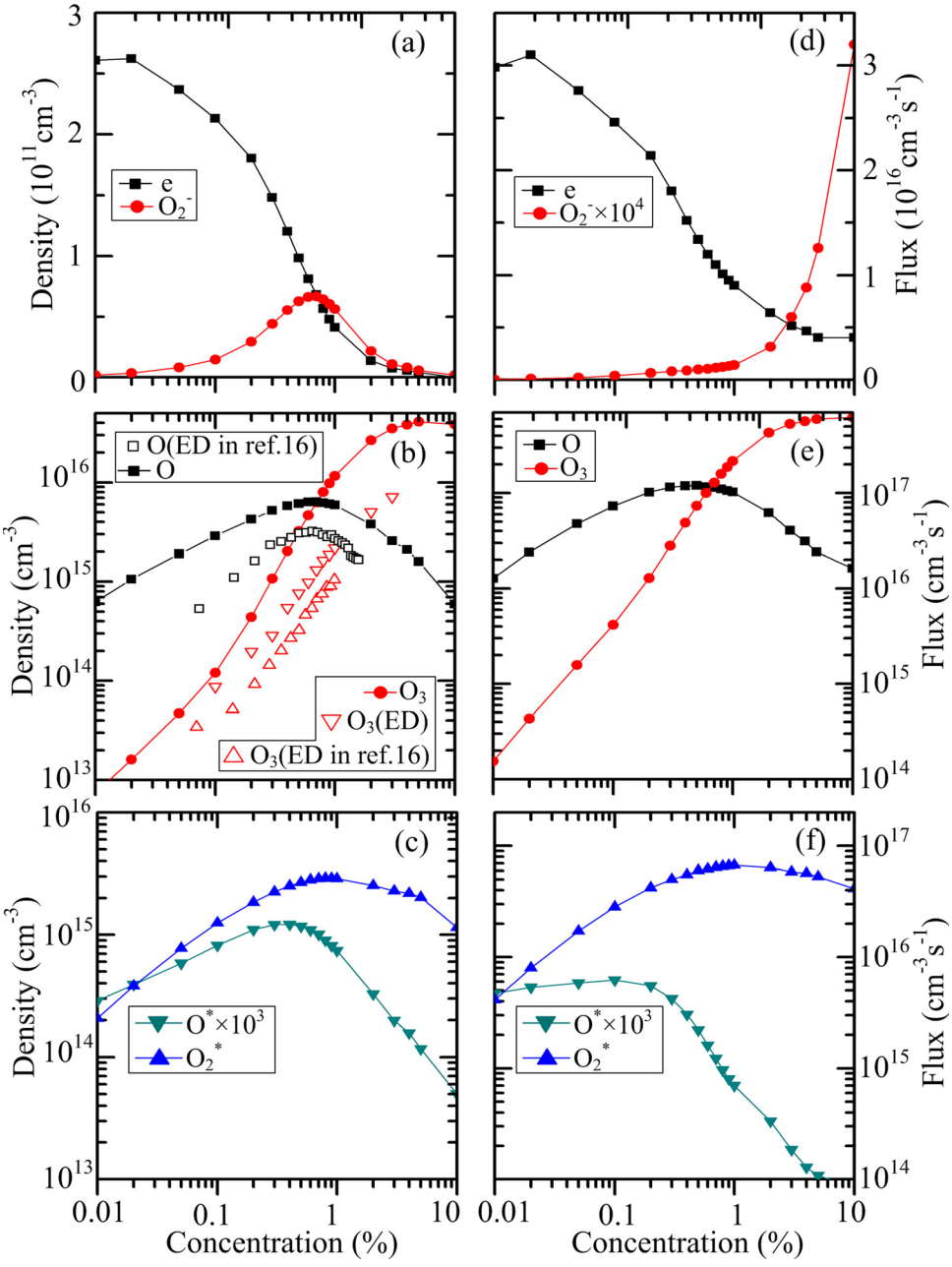

FIG. 3. The densities (time and spatial averaged) and wall fluxes (time averaged) of electron and important ROS as a function of oxygen concentration. ED: experiment data in this paper, ED in reference: the experiment data in corresponding references, others: numerical data.

peaking at $[O_2] = 1\%$, 1%, 0.7%, and 0.9%, respectively. It is noted that the power dissipations on the ROS production are closely related to their densities, as will be discussed later. Besides, the power dissipation on the production of vibrational excited species is significant in He + H_2 plasmas,[38] whereas it can be neglected in He + O_2 plasmas.

C. Wall fluxes of reactive species

It is desirable that reactive species can act on the treated sample efficiently and this is determined by plasma wall fluxes. However, wall fluxes of plasma species are difficult to be quantified experimentally and instead the time- and space-averaged densities are used as an indirect indicator. As shown in Fig. 3, the densities and wall fluxes of electron, O, O_2*, and O_3 share very similar dependence of the O_2 concentration, but this does not apply to O_2^- and O*. As suggested in our previous studies, only the species generated in the boundary layers of several to several hundred micrometers next to an electrode are effective for the supply of their wall fluxes.[18,19] The boundary layers for both O_2^- and O* have thickness of a few micrometers, in which the electron density and the electron temperature are much different to those in the plasma bulk (see Fig. 1), suggesting very different production mechanisms. Take O_2^- as an example, the generation is dominated by $O_3^- + O \rightarrow O_2^- + O_2$ in plasma bulk, whereas it is dominated by $e + O_2 + M \rightarrow O_2^- + M$ in the sheath (especially in the boundary layer). This is because the ozone has a much higher density in the bulk region. As a result, the average density of O_2^- increases and then decreases similar to that for O, but the wall flux of O_2^- keeps increase due to the increase of $[O_2]$ being larger than the drop of the electron density.

As shown in Fig. 3, the density and the wall flux of electrons reach their peaks both at $[O_2] = 0.02\%$. The initial rise is attributed to the enhancement of the Penning ionization of oxygen, and the subsequent fall is due to the increase of the electron attachment. The densities of O, O*, O_2*, O_2^- are found to peak at $[O_2] = 0.7\%$, 0.4%, 0.9%, and 0.7%, respectively, similar to their coupling powers as shown in Fig. 2(b). This implies that the densities of species are governed by their power dissipation, and that their production may be optimized by tuning the electrical power density. Experimental data of O_3 in Fig. 3 are measured with UV absorption spectroscopy, although it is lower than numerical data by up to 5 times, the trend is similar (see Fig. 3(b)). Moreover, experimental data of O and O_3 densities from literature have a similar trend to the numerical results.[8] In particular, the point at $[O_2] = 0.6\%$ for the maximum O density is the same for experimental and numerical data, even though the discharge conditions are somewhat different.

D. ROS generation and destruction mechanisms

In order to further understand the impact of the oxygen concentration on He + O_2 CAPs, the underlying chemistry for the generation and reduction of main ROS is illustrated in Fig. 4, for $[O_2] = 0.01\%$–10%. Because the chemistry is very complex, we consider here only the main reactions. As shown in Fig. 4, the ground state O is mainly generated by

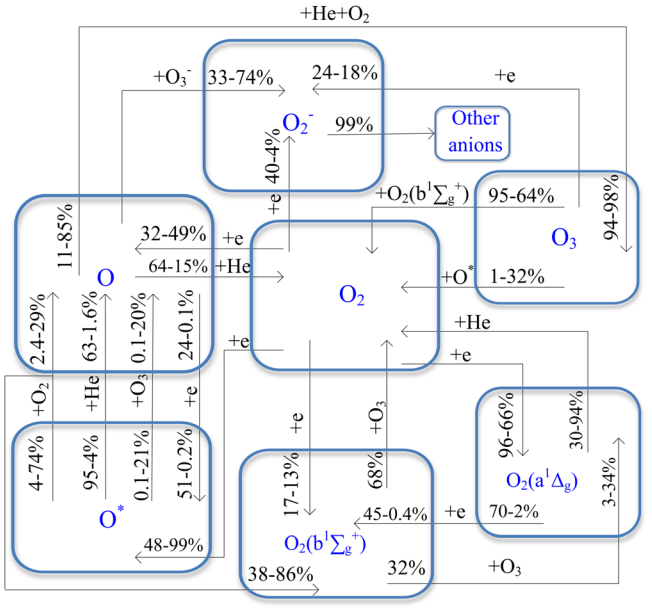

FIG. 4. The primary chemical processes for ROS and their contribution rates for the generation & destruction of specific species with respect to oxygen concentration from 0.01% to 10%. The percentage values near the start of the arrows represent the contribution rates for destruction, and the percentage values near the end of the arrows mean that for generation. The data representation like 48%–99% means the contribution rate increases from 48% to 99% as the increase of oxygen concentration from 0.01% to 10%.

electron dissociation of oxygen and the collision relaxation of O* via He ($[O_2] < 0.5\%$), oxygen ($[O_2] > 0.1\%$) and ozone ($[O_2] > 0.5\%$), and reduced by electron impact excitation ($[O_2] < 0.3\%$) and three-body reactions like O + O + He → O_2 + He and O + O_2 + He → O_3 + He. As for O*, it is mainly generated by electron impact excitation of O ($[O_2] < 0.5\%$) and O_2, whereas it is reduced by collision relaxation with He ($[O_2] < 0.5\%$), O_2 ($[O_2] > 0.05\%$), or O_3 ($[O_2] > 0.5\%$). $O_2(a^1\Delta_g)$ is mainly generated by electron impact with O_2 and the relaxation of $O_2(b^1\sum_g^+)$ via O_3, whilst it is mainly destructed by quenching via He and the step-wise excitation ($[O_2] < 0.5\%$). $O_2(b^1\sum_g^+)$ is mainly generated by electron impact excitation of O_2 and $O_2(a^1\Delta_g)$ ($[O_2] < 0.5\%$), and also by $O(^1D) + O_2 \rightarrow O + O_2(b^1\sum_g^+)$. O_3 is generated by O + O_2 + He → O_3 + He. The reactions between $O_2(b^1\sum_g^+)$ and O_3 form the main pathway for the destruction of both species. O_2^- is primarily generated by $O_3^- + O \rightarrow O_2^- + O_2$ and electron attachment ($e + O_2 + He \rightarrow O_2^- + He$ and $e + O_3 \rightarrow O_2^- + O$), and destructed by ion transfer. On the whole, there are strong chemistry links among the ROS which are strongly and sensitively dependent on the oxygen concentration.

IV. CONCLUSIONS

In summation, the additive of oxygen has been shown to significantly impact on the dynamics and the behaviors of ROS of He + O_2 CAPs when $[O_2] \geq 0.1\%$. Due to a dramatic increase of electron attachment with the oxygen concentration from $[O_2] = 0.1\%$ to 10%, the electron density decreases by more than one order of magnitude. As a result, the electron heating drops and in turn the ion joule heating becomes

dominant. The electron temperature decreases in the sheath but increases in the plasma bulk, resulting in the discharge transition from the γ mode to the α mode. The power dissipation for the production of O, O*, O_2*, O_2^- first increases and then decreases, and this is reflected in the trend of their average densities that peak in the narrow range of $[O_2] = 0.4\%–0.9\%$. Normally, the wall flux of a specific species can be described by its average density, but this does not apply to O* and O_2^-, because their boundary layers are very thin of $\sim\mu$m and their production mechanisms are much different in the narrow boundary layer to that in the plasma bulk. For the whole plasma, the main generation and destruction processes for ROS are quantified in this paper with respect to the oxygen concentration from 0.01% to 10%, and all of the processes are found to be strongly dependent on the oxygen concentration.

ACKNOWLEDGMENTS

This work was supported by the National Science Foundation of China (No. 51221005), the State Key Laboratory of Electrical Insulation and Power Equipment (No. EIPE14312).

[1]E. G. II, M. D. Barankin, P. C. Guschl, and R. F. Hicks, Plasma Processes Polym. **7**, 482 (2010).
[2]E. A. Ermolaeva, A. F. Varfolomeev, M. Y. Chernukha *et al.*, J. Med. Microbiol. **60**, 75 (2011).
[3]M. G. Kong, G. Kroesen, G. Morfill, T. Nosenko, T. Shimizu, J. van Dijk, and J. L. Zimmermann, New J. Phys. **11**, 115012 (2009).
[4]T. Martens, A. Bogaerts, W. J. M. Brok, and J. V. Dijk, Appl. Phys. Lett. **92**, 041504 (2008).
[5]X. H. Yuan and L. L. Raja, Appl. Phys. Lett. **81**, 814 (2002).
[6]J. Park, I. Henins, H. W. Herrmann, G. S. Selwyn, J. Y. Jeong, R. F. Hicks, D. Shim, and C. S. Chang, Appl. Phys. Lett. **76**, 288 (2000).
[7]N. Knake, K. Niemi, S. Reuter, V. Schulz-von der Gathen, and J. Winter, Appl. Phys. Lett. **93**, 131503 (2008).
[8]D. Ellerweg, J. Benedikt, A. von Keudell, N. Knake, and V. Schulz-von der Gathen, New J. Phys. **12**, 013021 (2010).
[9]G. Park, H. Lee, G. Kim, and J. K. Lee, Plasma Processes Polym. **5**, 569 (2008).
[10]D. X. Liu, X. H. Wang, M. Z. Rong, F. Iza, M. G. Kong, and P. Bruggeman, Plasma Processes Polym. **7**, 846 (2010).
[11]J. He and Y. T. Zhang, Plasma Processes Polym. **9**, 919 (2012).
[12]W. D. Zhu and J. L. Lopez, Plasma Sources Sci. Technol. **21**, 034018 (2012).
[13]S. G. Wang and J. Wan, IEEE Trans. Plasma Sci. **37**, 551 (2009).
[14]V. Léveillé and S. Coulombe, Plasma Processes Polym. **3**, 587 (2006).
[15]N. Georgescu, C. P. Lungu, A. R. Lupu, and M. Osiac, IEEE Trans. Plasma Sci. **38**, 3156 (2010).
[16]J. L. Walsh, D. X. Liu, F. Iza, M. Z. Rong, and M. G. Kong, J. Phys. D: Appl. Phys. **43**, 032001 (2010).
[17]A. J. Yang, X. H. Wang, M. Z. Rong, D. X. Liu, F. Iza, and M. G. Kong, Phys. Plasmas **18**, 113503 (2011).
[18]D. X. Liu, A. J. Yang, X. H. Wang, M. Z. Rong, F. Iza, and M. G. Kong, J. Phys. D: Appl. Phys. **45**, 305205 (2012).
[19]A. J. Yang, M. Z. Rong, X. H. Wang, D. X. Liu, and M. G. Kong, J. Phys. D: Appl. Phys. **46**, 415201 (2013).
[20]D. Liu, F. Iza, and M. G. Kong, IEEE Trans. Plasma Sci. **36**, 952 (2008).
[21]D. W. Liu, F. Iza, and M. G. Kong, Plasma Processes Polym. **6**, 446 (2009).
[22]B. Halliwell and J. M. C. Gutteridge, *Free Radicals in Biology and Medicine*, 4th ed. (Clarendon Press, Oxford, 2007).
[23]M. A. Malik, A. Ghaffar, and S. A. Malik, Plasma Sources Sci. Technol. **10**, 82 (2001).
[24]T. Suzuki, T. Saburi, R. Tokunami, H. Murata, and Y. Fujii, Thin Solid Films **506**, 342 (2006).
[25]A. N. Bhoj and M. J. Kushner, Plasma Sources Sci. Technol. **17**, 035024 (2008).
[26]J. Waskoenig, K. Niemi, N. Knake, L. M. Graham, S. Reuter, V. Schulz-von der Gathen, and T. Gans, Plasma Sources Sci. Technol. **19**, 045018 (2010).
[27]Q. Wang, D. J. Economou, and V. M. Donnelly, J. Appl. Phys. **100**, 023301 (2006).
[28]X. H. Yuan and L. L. Raja, IEEE Trans. Plasma Sci. **31**, 495 (2003).
[29]Y. Sakiyama and D. B. Graves, Plasma Sources Sci. Technol. **18**, 025022 (2009).
[30]K. Niemi, J. Waskoenig, N. Sadeghi, T. Gans, and D. O'Connell, Plasma Sources Sci. Technol. **20**, 055005 (2011).
[31]H. W. Ellis, R. Y. Pai, E. W. McDaniel, E. A. Mason, and L. A. Viehland, At. Data Nucl. Data Tables **17**, 177 (1976).
[32]G. J. M. Hagelaar and L. C. Pitchford, Plasma Sources Sci. Technol. **14**, 722 (2005).
[33]P. F. Kurunczi, J. Guha, and V. M. Donnelly, Phys. Rev. Lett. **96**, 018306 (2006).
[34]M. Moravej, X. Yang, G. R. Nowling, J. P. Chang, and R. F. Hicks, J. Appl. Phys. **96**, 7011 (2004).
[35]K. McKay, D. X. Liu, F. Iza, M. Z. Rong, and M. G. Kong, IEEE Trans. Plasma Sci. **39**, 2138 (2011).
[36]D. W. Liu, F. Iza, and M. G. Kong, Appl. Phys. Lett. **95**, 031501 (2009).
[37]D. D. Monahan and M. M. Turner, Plasma Sources Sci. Technol. **17**, 045003 (2008).
[38]D. X. Liu, F. Iza, X. H. Wang, Z. Z. Ma, M. Z. Rong, and M. G. Kong, Plasma Sources Sci. Technol. **22**, 055016 (2013).